Journal of Nuclear Materials 501 (2018) 224–233

Contents lists available at ScienceDirect

Journal of Nuclear Materials

journal homepage: www.elsevier.com/locate/jnucmat

Radiolytic stability of gibbsite and boehmite with adsorbed water

Patricia Huestis [a, b], Carolyn I. Pearce [c], X. Zhang [c], Alpha T. N'Diaye [d], Kevin M. Rosso [c], Jay A. LaVerne [a, b, *]

[a] Radiation Laboratory, University of Notre Dame, Notre Dame, IN 46556, USA
[b] Department of Physics, University of Notre Dame, Notre Dame, IN 46556, USA
[c] Pacific Northwest National Laboratory, Richland, WA, USA
[d] Advanced Light Source, Lawrence Berkeley National Laboratory, Berkeley, CA, USA

ARTICLE INFO

Article history:
Received 10 November 2017
Received in revised form
22 January 2018
Accepted 23 January 2018
Available online 6 February 2018

ABSTRACT

Aluminum oxyhydroxide (boehmite, AlOOH) and aluminum hydroxide (gibbsite, $Al(OH)_3$) powders with adsorbed water were irradiated with γ-rays and 5 MeV He ions (α-particles) in order to determine overall radiation stability and chemical modification to the surface. No variation in overall phase or crystallinity due to radiolysis was observed with X-ray diffraction (XRD) and Raman spectroscopy for doses up to 2 MGy with γ-rays and 175 MGy with α-particles. Temperature programed desorption (TPD) of the water from the surface to the gas phase indicated that the water was chemisorbed and strongly bound. Water adsorption sites are of similar energy for both gibbsite and boehmite. Observation of the water adsorbed on the surface of gibbsite and boehmite with diffuse reflectance infrared Fourier transform spectroscopy (DRIFTS) showed broad peaks at 3100-3600 cm^{-1} due to OH stretching that slowly decreased on heating to 500 °C, which corresponds well with the water vapor evolution observed with TPD. Both materials were found to be amorphous following heating to 500 °C. X-ray photoelectron spectroscopy (XPS) indicated surface reduction of Al(III) to Al metal on radiolysis with α-particles. Complete loss of chemisorbed water and the formation of bulk O atoms was observed following radiolysis with α-particles.

1. Introduction

Aluminum oxyhydroxide (boehmite, AlOOH) and aluminum hydroxide (gibbsite, $Al(OH)_3$) are prominent components in nuclear waste and ultimately must be considered in separation streams before final vitrification and storage as glass. Low temperature water cooled reactors and test reactors use aluminum cladding [1] that becomes a component of the waste following decommissioning, and legacy waste at Hanford contains significant amounts of aluminum compounds from cladding and reprocessing [2]. Excessive amounts of aluminum in waste separation streams decreases the chemical stability of the vitrified glass through the precipitation of nepheline, $NaAlSiO_4$ [3,4]. Reduction in the amount of vitrified waste can be achieved by removal of the aluminum, but radiolysis by the decay of the radioactive components in the mixture can lead to significant chemical changes, particularly at the solid surfaces, that complicate chemical extraction. This work focuses on the radiolytic modification of boehmite and gibbsite under relatively mild conditions of adsorbed water in order to determine fundamental radiolytic processes occurring on the particle surfaces absent the challenges expected from the rather harsh environments present in waste streams of storage tanks.

Radiolytic studies on gibbsite and boehmite have been performed, but the focus of this previous work was mainly on the production of molecular hydrogen, H_2, from dried samples [5,6]. Both studies found that H_2 production was greater with boehmite than with gibbsite, which can be due to a number of reasons including the suggested difference in energy to make the precursor H atom. Electron paramagnetic resonance (EPR) studies found oxygen centered defect sites following radiolysis, but little other characterization of these materials has been performed [5]. On the other hand, extensive characterization of the radiolysis of alumina (Al_2O_3) in association with various amounts of water has been performed [7]. This latter work determined that H_2 production from adsorbed water and from various percent water slurries was higher than that expected from bulk water. Changes to the bulk alumina was not observed in radiolysis, but surface reduction of

* Corresponding author. Radiation Laboratory, University of Notre Dame, Notre Dame, IN 46556, USA.
E-mail address: laverne.1@nd.edu (J.A. LaVerne).

https://doi.org/10.1016/j.jnucmat.2018.01.043
0022-3115/

Al(III) to Al metal was suggested by spectroscopic techniques. Radiolytic modification of gibbsite and boehmite surfaces has not been examined.

In this work, the behavior of gibbsite and boehmite powders was examined in the γ-radiolysis of these particles with adsorbed water. Studies were also performed with 5 MeV He ion irradiation to simulate α-particle radiolysis and to give large local doses. Gamma rays lose energy mainly by Compton effects to produce β-rays, which along with alpha particles are the two major sources of radiation observed in tank waste [8]. Bulk phase and crystallinity characteristics were determined using X-ray diffraction (XRD). Surface characterization of the powders was performed using nitrogen adsorption and the Brunauer – Emmett – Teller (BET) methodology to determine porosity and particle size. Temperature programmed diffuse reflection infrared Fourier transform spectroscopy (DRIFTS) in conjunction with temperature programmed desorption (TPD) was used to examine water adsorbed on and desorbed from the surface, respectively. Raman spectroscopy gave information on the bulk chemical composition, while X-ray photoelectron spectroscopy (XPS) and X-ray absorption spectroscopy (XAS) were used for analysis of chemical changes to the surfaces.

2. Experimental section

2.1. Synthesis of gibbsite

The experimental protocol for synthesis of gibbsite was reported in detail in Zhang et al. [9]. Firstly, $Al(NO_3)_3 \cdot 9H_2O$ (≥98%, Sigma-Aldrich) was dissolved in deionized water while stirring to form a homogeneous solution with an Al concentration of 0.25 M at room temperature, followed by adding 1 M NaOH (≥98%, Sigma-Aldrich) aqueous solution to adjust the pH to around 5.0. After continuous stirring for 1 h, the solution was centrifuged to collect gel-like condensates. The gel was washed with deionized water three times to remove soluble salts, dispersed into pure water, and transferred to a 100 mL Teflon-lined Parr bomb autoclave. Gel concentration (defined as Al concentration) was 0.5 M and volume of the gel solution is 80 mL. The Parr bomb was heated in an electric oven at 80 °C for 3 days and the resulting white product was recovered by centrifuging and washing with deionized water three times. The solid sample obtained was dried in an oven at 80 °C overnight.

2.2. Synthesis of boehmite

The experimental protocol for synthesis of boehmite was reported in detail in Zhang et al. [9]. Aqueous solution of 1 M NaOH was added to 0.25 M $Al(NO_3)_3 \cdot 9H_2O$ to adjust the pH to around 10. After continuous stirring for 1 h, the solution was centrifuged to collect gel-like precipitates. The gel was washed with deionized water three times to remove soluble salts and then the gel was dispersed into deionized water. The pH of the solution was adjusted to around 12 using 1 M NaOH and then transferred into a 100 mL Teflon-lined Parr bomb. Gel concentration was 0.1 M and volume of the gel solution was 80 mL. The Parr bomb was heated in an electric oven at 200 °C for 2 days and the resulting white product was recovered by centrifuging and washing with deionized water three times. The solid sample obtained was dried in oven at 80 °C overnight.

2.3. Particle characterization

Nitrogen adsorption obtained from a Quantachrome Autosorb 1 and the Brunauer-Emmett-Teller (BET) methodology were used to determine the specific surface area, porosity, and size of the particles. Two complimentary techniques were used to observe water and contaminants present on the surface: temperature programmed desorption (TPD) and diffuse reflectance infrared Fourier transform spectroscopy (DRIFTS). The TPD measurements were performed on sample masses of approximately 100 mg that were deposited into a custom cell containing a cartridge heater. The cell was heated from 25 °C to 500 °C at a rate of 5 °C/min while the desorbing gases were monitored using a Pfeiffer Prisma quadrupole mass spectrometer. Mass to charge ratios of 14, 15, 16, 18, 28, 32, 40, and 44 were all scanned throughout the run. The largest signal was from water which has a mass to charge ratio of 18. The background measurement was done on an empty cell before each run and was subtracted from the sample spectrum. DRIFTS measurements were obtained using a Bruker Vortex 70 with a Harrick Praying Mantis high temperature cell. The materials were found to absorb strongly in the IR range and were therefore mixed at a 1:1 ratio with KBr to obtain a cleaner signal. The background spectrum was taken of pure KBr.

The crystalline structure was probed using powder X-ray diffraction (XRD). The XRD measurements were taken using a Bruker D8 Advance Davinci Powder X-ray Diffractometer that uses Cu-Kα X-rays. Scans were taken over the 2θ range of 10°–90° at an increment of 0.015°. The samples were rotated at a rate of 15 rotations per minute to increase the signal and prevent damage that might occur from the X-ray beam. Scanning electron microscopy (SEM) was performed using a Magellan 400 FESEM on particles attached to an aluminum stub and coated with 1.5 nm iridium using a sputter coater.

Chemical analysis was completed using Raman spectroscopy, X-ray photoelectron spectroscopy (XPS) and X-ray absorption spectroscopy (XAS). Raman measurements were taken with a Jasco Micro-Raman Spectrometer MRS-5100 using a 532 nm laser that had a power of about 4–5 mW. The resolution of the setup was 1.8 cm^{-1} and had an estimated sampling depth of about 1 μm. XPS measurements were taken with a PHI VersaProbe II X-ray photoelectron spectrometer using a monochromatic Al-Kα X-ray source and a hemispherical electron energy analyzer. Low resolution survey scans were taken to monitor impurities and obtain relative composition percentages using a pass energy of 187.85 eV. High resolution scans were taken of elements of interest using a pass energy of 23.5 eV. Samples for XPS analysis were first deposited onto an aluminum SEM stub and affixed using a conductive double stick carbon tab. The stub with the material was then coated in a thin layer of iridium to mitigate differential charging effects.

X-ray absorption near edge structure (XANES) at the Al and O K-edges and extended X-ray absorption fine structure (EXAFS) data for Al were collected on Beamline 6.3.1.1 at the Advanced Light Source (Berkeley, CA). A powdered sample was pressed into indium foil and mounted onto a copper sample probe using silver paint. The XAS signal was monitored at room temperature in total-electron-yield (TEY) mode with an effective probing depth of ~ 4 nm [10]. A reference spectra of corundum (Al_2O_3) was used to calibrate the energy scale [11]. The photon energy resolution values for Al K-edge spectroscopy was 0.75 eV. The XANES and EXAFS data were analyzed using the Athena interface to the IFEFFIT program [12].

2.4. Gamma irradiations

The samples were baked in a vacuum oven at 105 °C for 4 h and allowed to cool under vacuum for an additional 3 h. After cooling, the materials were placed in a 53% relative humidity chamber made from a saturated slurry of $Mg(NO_3)_2$ to allow the materials to adsorb water over the course of several days. The materials were

then transferred to Pyrex test tubes (10 cm long x 10 mm diameter) and placed on a vacuum rack to degas three times using a freeze-pump-thaw method. Following degassing, the sample vials were flame-sealed and irradiated at room temperature using a contained Shepard ^{60}Co source located at the University of Notre Dame Radiation Laboratory, which had a dose rate in February 2017 of 121 Gy/min as determined by Fricke dosimetry. Periodic corrections were made for changes in dose rate due to natural decay. The samples were irradiated up to a total dose of 2 MGy and the sample vials were cracked open to retrieve the powder for post-irradiation analysis.

2.5. Helium ion irradiations

Particles prepared as for gamma radiolysis were deposited on to aluminum SEM stubs using a carbon double sided tab from Ted Pella to affix the material to the stub. Irradiations of the stubs were performed using $^{4}He^{2+}$ ions from a 10 MV FN Tandem Van de Graaff accelerator in the Nuclear Science Laboratory of the University of Notre Dame Physics Department. Ion energies incident to the samples were 5 MeV with energy loss to windows determined using standard stopping power compilations [13]. The samples were irradiated in a nitrogen-flushed environment. The beam diameter was 6.4 mm and the samples were irradiated to a fluence of 1×10^{15} ions/cm^2 as determined by integration of the beam current on target. The total dose per sample was about 175 MGy and beam currents were kept sufficiently low to ensure no sample heating occurred.

3. Results and discussion

3.1. Characterization of gibbsite and boehmite bulk

The gibbsite and boehmite particles were synthesized in order to control purity and to ensure particle integrity by optimizing established synthesis techniques towards these property variables [9]. The SEM images of the powders are shown in Fig. 1 while the observed XRD patterns of the pristine particles are shown in Fig. 2 and match exactly with that expected from the instrument library. Gibbsite consists of planes of aluminum ions each between two layers of hydroxyl ions while boehmite is made up of double layers of oxygen/hydroxyl octahedra partially filled with aluminum ions [14]. No obvious impurities in the particles are detected in the diffraction patterns. Radiolysis with γ-rays up to a dose of 2 MGy shows no variation in the diffraction patterns, which suggests that

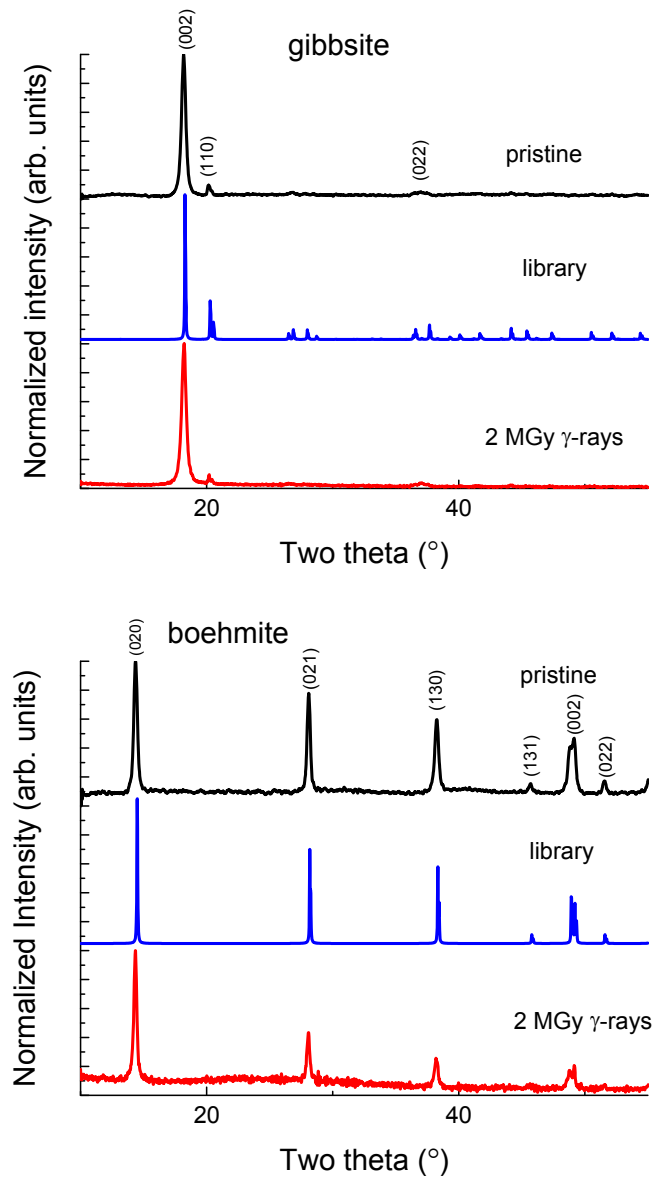

Fig. 2. X-ray diffraction (XRD) patterns of gibbsite and boehmite for pristine powders, instrument library reference and following 2 MGy γ-ray radiolysis.

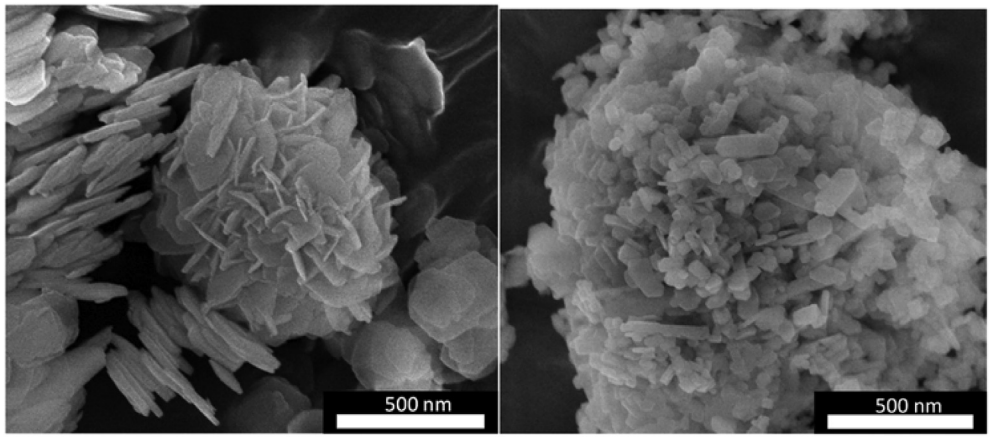

Fig. 1. SEM images of gibbsite (left) and boehmite (right).

the bulk materials have considerable radiation stability with regard to their phase and crystallinity. Similar results have been observed with alumina [7] and are expected since photons, and the secondary electrons they produce, exert little momentum transfer to displace atoms.

Nitrogen adsorption and desorption was used to determine particle size and porosity. Desorption plots of nitrogen track almost identically over those for adsorption for both gibbsite and boehmite suggesting smooth particles with insignificant porosity that may affect the surface chemistry. Specific surface areas obtained using the BET methodology are 42.3 m^2/g and 46.8 m^2/g for gibbsite and boehmite, respectively. These surface areas correspond to particle diameters of 59 nm and 42 nm, respectively, assuming spherical particles. However, the particles are definitely not spherical and these diameters are only listed to give a relative size. SEM images show a stacked platelet configuration so there is considerable deviation from spherical symmetry.

Raman spectroscopy is a rather straightforward technique for the identification of materials from their bonding. At the wavelengths used in this work, the spectroscopy probes at depths of up to a micron. Since the particles are only 50 nm in diameter, Raman spectroscopy is essentially probing the bulk materials. Raman spectra for gibbsite and boehmite have been both measured and calculated [14,15]. The Raman spectra for gibbsite and boehmite are shown in Fig. 3 at low wavenumbers and in Fig. 4 for high wavenumbers. At the low wavenumbers the gibbsite and boehmite spectra are almost identical with that in the literature [14]. The major bands in gibbsite at 539 cm^{-1} and 569 cm^{-1} are ascribed to Al-O-Al deformation, the major band at 321 cm^{-1} with a shoulder at 307 cm^{-1} is due to the Al-O stretch, while the minor bands in the range of 900–1050 cm^{-1} are attributed to hydroxyl deformation modes [14].

The low wavenumber Raman spectrum for boehmite is simpler than that for gibbsite. The bands in the region of 400–800 cm^{-1} are attributed to hydroxyl translation modes while the very weak bands in the 900 to 1050 cm^{-1} region are due to hydroxyl deformation modes [14]. The strong peak at 361 cm^{-1} with a shoulder at 339 cm^{-1} is probably due to the Al-O stretching vibration.

At high wavenumbers the Raman spectra are dominated by the OH stretching modes. The main peaks for gibbsite are at 3359, 3432, 3522, and 3615 cm^{-1}, which agree almost exactly with previous work [14]. Boehmite has somewhat weaker peaks at 3112 and 3232 cm^{-1}, which agree with previous work [14], and smaller peaks at 3423 and 3546 cm^{-1}. These broad peaks for boehmite are probably due to surface hydroxyl stretching modes. Gibbsite will have stretching modes of hydroxyl groups internal to the material and the band at 3354 cm^{-1} is probably due to hydrogen bonds between the layers while and the bands at 3432 cm^{-1} and 3522 cm^{-1} are due to hydrogen bonds in the same plane.

Irradiation with γ-rays to 2 MGy and α-particles to 175 MGy show little variation in the low wavelength region for both gibbsite and boehmite with the possible exception of a slight decrease in the hydrogen deformation modes between 900 and 1050 cm^{-1}. These sites could be loss in the radiolytic formation of H_2 from these compounds [5,6].

3.2. Physical characterization of gibbsite and boehmite surfaces

Water is well known to dissociate and chemisorb to metal oxide surfaces [16]. The result is a surface of OH groups that will be infrared active. Of course, gibbsite and boehmite have inherent OH groups within their bulk. Distinguishing the difference between chemisorbed water and bulk OH groups is a challenge. Infrared spectra of gibbsite are shown in Fig. 5 while those for boehmite in Fig. 6. Broad physisorbed water peaks due to OH stretching are

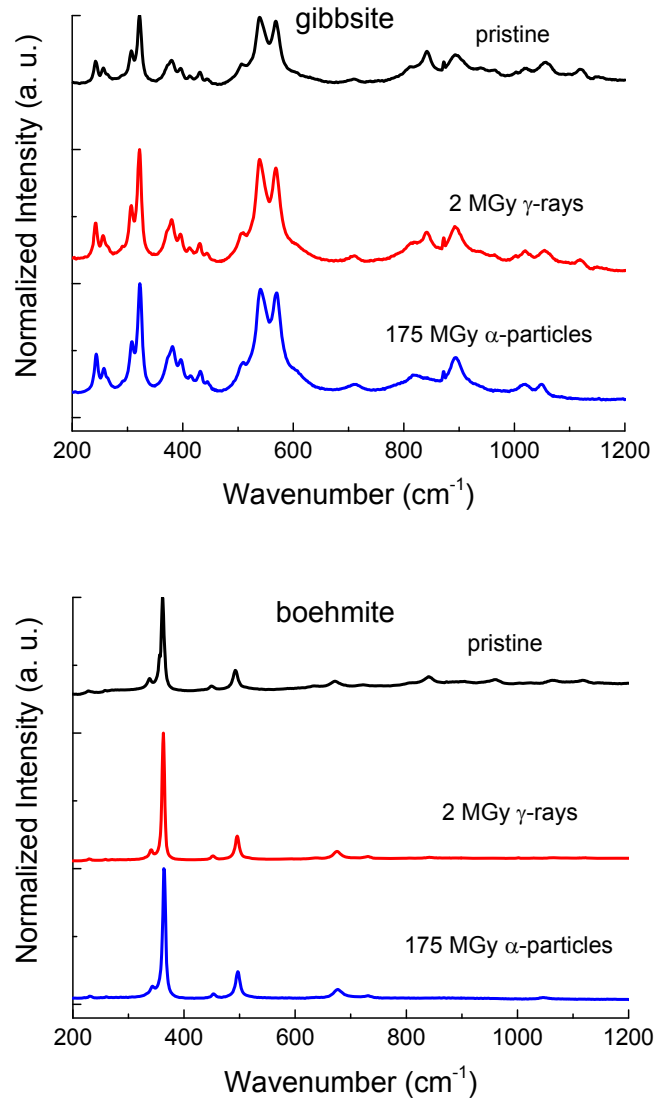

Fig. 3. Raman spectra of pristine gibbsite and boehmite in the low wavenumber region and for these materials irradiated to 2 MGy with γ-rays and 175 MGy with 5 MeV He ions (α-particles).

observed at 3400-3600 cm^{-1} for gibbsite and 3100-3300 cm^{-1} for boehmite. Bending modes of the OH groups are observed at 1000 cm^{-1} for gibbsite and at 1100 cm^{-1} for boehmite. Structural identification associated with these peaks has been proposed elsewhere [17,18]. On heating the samples from 25 to 500 °C a general decrease in the intensity of the physisorbed peaks are observed. The residual peaks at 500 °C are due to the chemisorbed OH groups at 3560 cm^{-1} for the boehmite, and 3570 cm^{-1} for gibbsite. An additional peak at 3225 cm^{-1} for gibbsite is probably due to internal OH stretching. The reflectances for the main peaks at 3500 and 3100 cm^{-1} for gibbsite and boehmite, respectively, are given as a function of temperature in the lower panels of Figs. 5 and 6 for gibbsite and boehmite, respectively. A rather dramatic shift in the reflectance is observed between 200 and 250 °C for gibbsite and 400–500 °C for boehmite. Reducing the temperature back to 25 °C results in the respective dashed lines in upper panels of the figures. Each of these dashed lines is significantly different from the original material. XRD patterns of the heated samples show complete amorphization of the gibbsite [19]. The XRD pattern of the post-heated boehmite is almost completely amorphous but there are

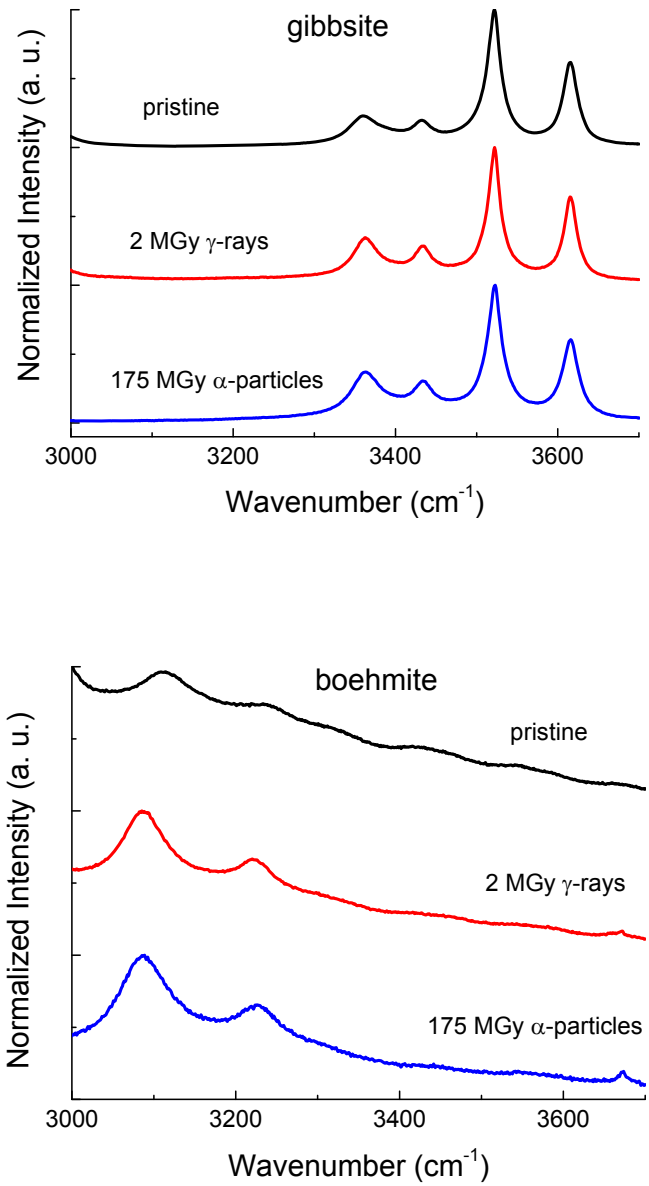

Fig. 4. Raman spectra of pristine gibbsite and boehmite in the high wavenumber region and for these materials irradiated to 2 MGy with γ-rays and 175 MGy with 5 MeV He ions (α-particles).

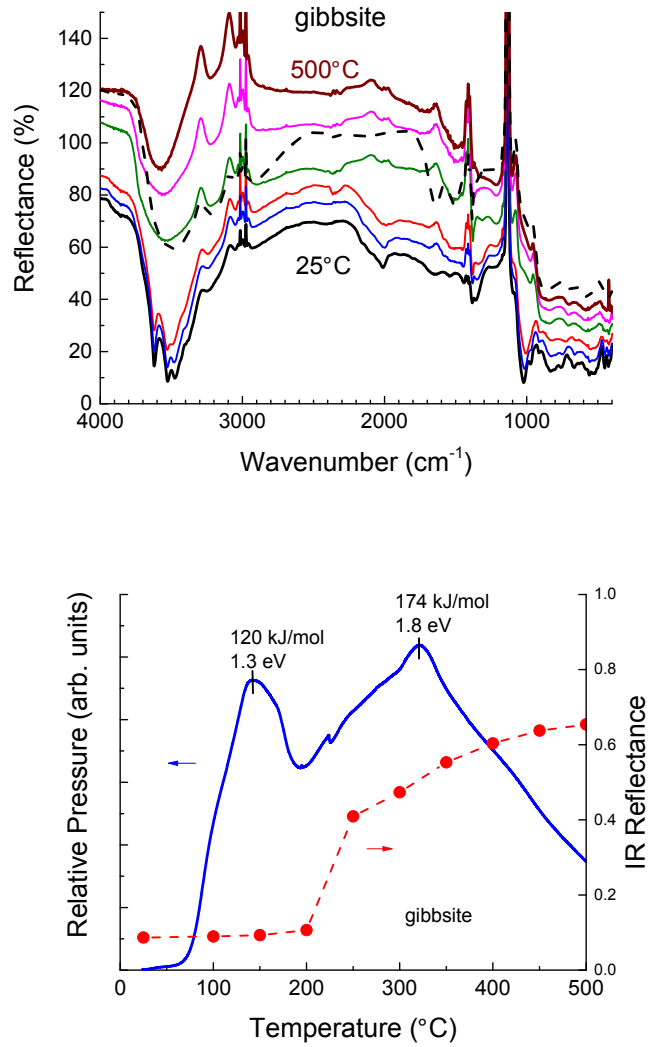

Fig. 5. Upper: DRIFTS spectra of gibbsite at 25, 100, 200, 300, 400 and 500 °C (solid lines) and at 25 °C following heating to 500 °C (dashed line). Lower: Temperature programmed desorption (TPD) of water from gibbsite (left scale) and IR reflectance at 3500 cm^{-1} as a function of temperature.

residual peaks that match alumina. The gibbsite was too far converted to make any observation on intermediate species, but the data appears to show that boehmite is heat transformed to alumina. A previous study using temperature gravimetric analysis (TGA) found extensive dehydroxylation of gibbsite at about 200 °C, but that work also suggested the same phenomenon occurs in boehmite at 250 °C, which is considerably lower temperature than that observed here [20]. Irradiations with α-particles did not extend to high displacements per atom, DPA, but one would expect amorphization to eventually occur at higher fluences. Heavier ions are expected to lead to amorphization because of the influence of nuclear or ballistic interactions with atoms of the medium [8]. Atomic displacement or complete amorphization of surfaces can have a profound effect on the chemical characteristics of gibbsite and boehmite particles and on the interactions between particles. The radiolysis of gibbsite and boehmite with heavier ions and in a variety of environments will be performed in the future.

The DRIFTS spectra of both gibbsite and boehmite are sensitive to the water that is on the powder surfaces. TPD studies monitor water that has desorbed from the surface, so these two techniques are very complementary for specifically probing water-surface interactions. The observed TPD for gibbsite is given in Fig. 5 while that for boehmite is in Fig. 6. A significant loss of water is observed at about 75 °C for gibbsite followed by peaks at about 140 and 320 °C. These peaks correspond to desorption energies of 1.3, and 1.8 eV, calculated using Redhead's method [21]. Energies this high suggest that chemisorbed water is evolving from the surface, since the energies are higher than the desorption energy for physisorbed water, 0.35 eV [22]. However, the large change in the reflectance in the range of 200–250 °C corresponds to a major phase or crystallinity change in the compound so the higher energy (temperature) peak is due to something that is not crystalline gibbsite. Boehmite shows two desorption peaks at 180 and 310 °C, which correspond to energies of 1.4 and 1.8 eV, respectively. The observed peaks of both gibbsite and boehmite have similar energies suggesting that the water on these surfaces is nearly identical, so the surface site energies must be very similar. As with gibbsite, there is a marked drop in the water desorption when the infrared reflectance

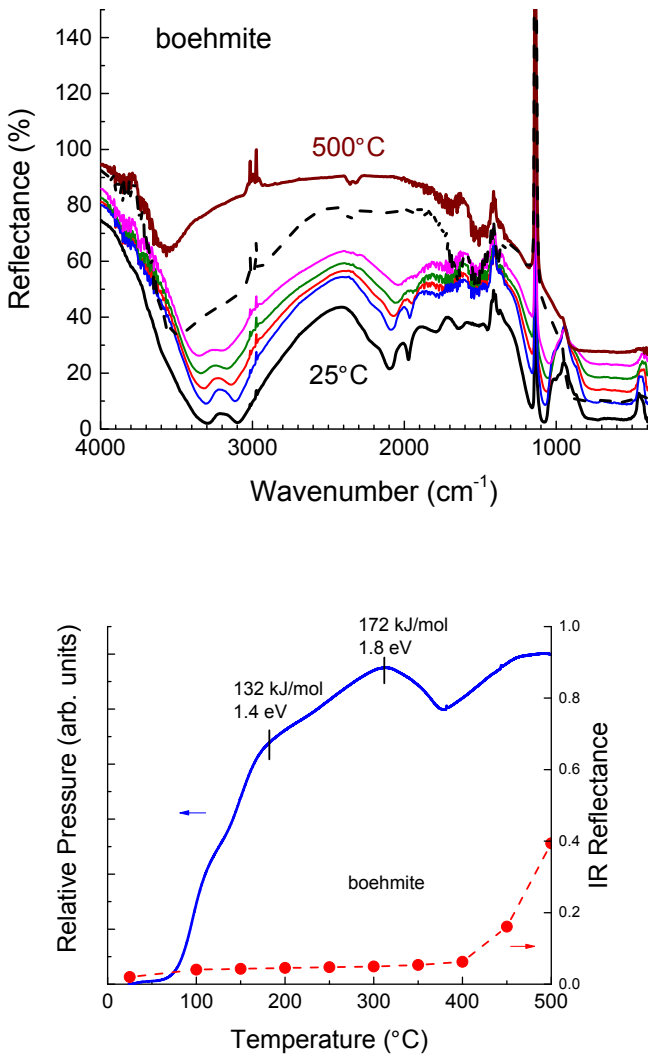

Fig. 6. Upper: DRIFTS spectra of boehmite at 25, 100, 200, 300, 400 and 500 °C (solid lines) and at 25 °C following heating to 500 °C (dashed line). Lower: Temperature programmed desorption (TPD) of water from boehmite (left scale) and IR reflectance at 3500 cm^{-1} as a function of temperature.

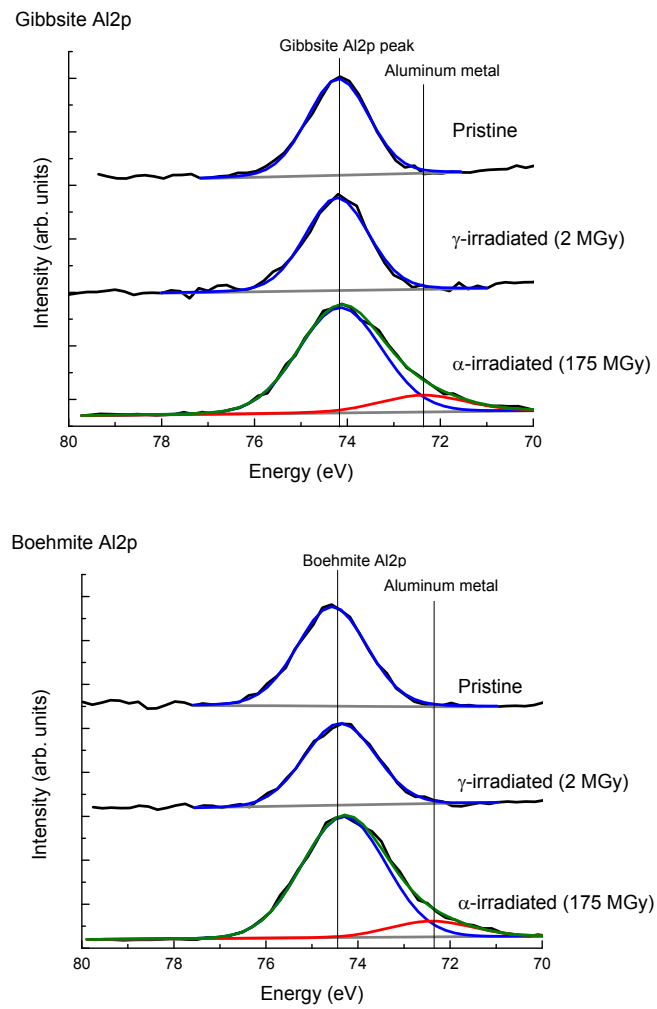

Fig. 7. XPS Al 2p spectra of pristine gibbsite and boehmite and of samples irradiated to 2 MGy with γ-rays and 175 MGy with α-particles.

suggests a major phase or crystallinity change is occurring.

The evolution of H_2 from gibbsite heated post radiolysis has been examined and further work on heating pre-radiolysis is underway. No attempt was made to examine the effects of radiolysis on the DRIFTS spectra because the samples were exposed to atmosphere before spectroscopic analysis allowing water to re-equilibrate with the surface.

3.3. Chemical characterization of gibbsite and boehmite surfaces

XPS measurements were used to analyze any changes to the surface composition and electronic state of surface atoms following irradiation. A survey scan from 1400 to 0 eV binding energy revealed no contamination other than inevitable adventitious carbon, which was used to charge correct the scans by setting the C-C 1s peak to 284.8 eV. Spectra of the Al 2p electrons are shown in Fig. 7 for both gibbsite and boehmite. The pristine gibbsite has a single peak at 74.2 eV, which corresponds to the aluminum bonding found in gibbsite [23]. Irradiating with γ-rays does not appear to alter the aluminum peak for gibbsite, but irradiations with α-particles show the appearance of a secondary peak at 72.3 eV. This peak could possibly be due to aluminum metal, which is reported at 72.7 eV by Konstadinidis et al. [24], suggesting that the α-particles reduced the surface of the gibbsite powder from Al(III) to aluminum metal. Similar results are seen for boehmite, which has a single peak at 74.4 eV for both the pristine and the γ-irradiated samples, and the introduction of an additional peak at 72.3 eV for the α-irradiated sample. Reduction of Al(III) to Al metal was suggested previously in the radiolysis of alumina, so this process is likely common to all aluminum oxides [7].

XPS O 1s spectra are shown in Fig. 8 for gibbsite and boehmite samples, which were analyzed for any changes in the peak structure. The pristine gibbsite sample has two contributions to the O 1s signal: one at 533.5 eV corresponding to adsorbed water on the surface (H-O-H), and one at 531.7 eV corresponding to the hydroxyl groups within the crystal structure (Al-O-H) [23]. The γ-irradiated sample again does not show any appreciable changes, which is corroborated with a lack of change in the Al 2p peak. The α-irradiated sample contains no contribution to adsorbed water, suggesting that water was removed during irradiation and the surface was altered enough to keep more water from adsorbing. In addition, two lower binding energy peaks appear following radiolysis with α-particles. The first peak is at 530.3 eV and can be attributed to bulk oxygen (Al-O-Al) [23]. This particular bond does not normally exist in gibbsite, and is therefore not seen in the pristine

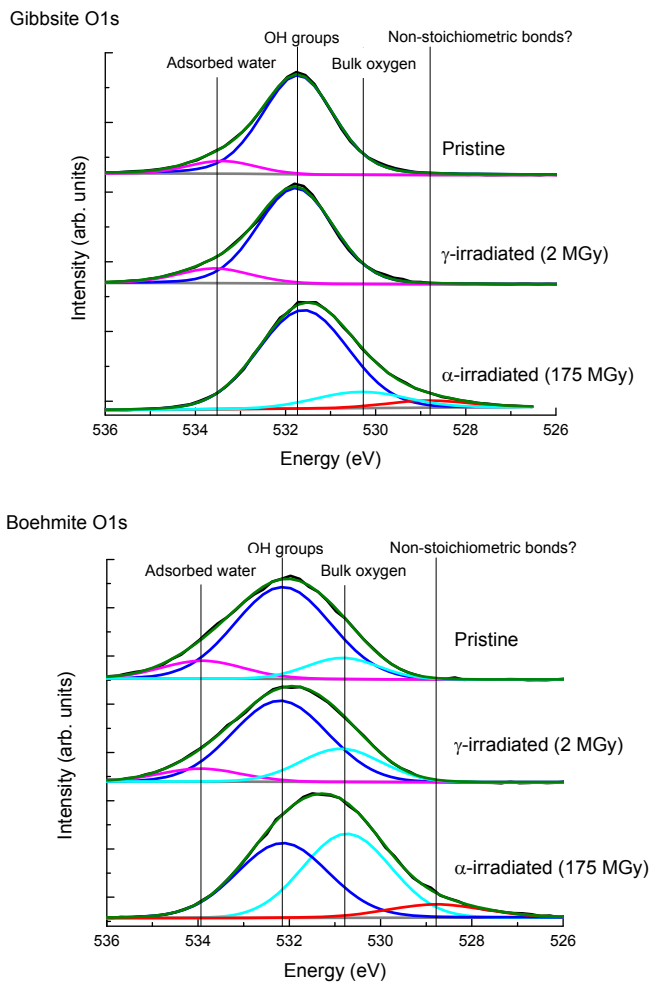

Fig. 8. XPS O 1S spectra of pristine gibbsite and boehmite and of samples irradiated to 2 MGy with γ-rays and 175 MGy with α-particles.

sample. The appearance of the bulk oxygen peak suggests that the sample has been reduced enough to start showing bonds indicative of boehmite or alumina. There is a further reduced peak at 528.8 eV which hints at a non-stoichiometric oxygen bond, but more work must be done to properly identify this peak.

The pristine boehmite sample shows three contributing peaks: one at 533.9 eV corresponding to adsorbed water on the surface (H-O-H), one at 532.2 eV corresponding to hydroxyl groups within the crystal structure (Al-O-H), and 530.8 eV corresponding to oxygen within the crystal structure (Al-O-Al) [23]. The γ-irradiated sample shows a relative decrease in adsorbed water and relative increase in bulk oxygen as can be seen from the tabulated values in Table 1. These changes are likely due to a smaller adsorbed water layer that allows for a deeper probing into the material. The relative ratio between the hydroxyl (Al-O-H) peak and the bulk oxygen (Al-O-Al) peak of boehmite should be about 1:1, but as shown in Table 1 even for the pristine sample this ration is about 4:1. Radiolysis with α-particles reduces this ratio to the expected 1:1 showing that significant rearrangement occurs during radiolysis. At this point, the adsorbed water peak is completely gone, which further supports the idea that the adsorbed water is masking the signal due to bulk oxygen. The α-irradiated boehmite sample also shows a peak at 528.8 eV, which is as yet unidentified.

Further analysis of the effects of γ-irradiation on gibbsite and boehmite samples was performed using Al K-edge XANES/EXAFS.

Table 1
Relative concentrations of different O and Al atoms as determined by XPS for pristine gibbsite and boehmite and for samples irradiated with γ-rays and α-particles.

Compound	Peak	Position (eV)	Attribution	Concentration (%)
Gibbsite Pristine	O1s − 1	533.42	Adsorbed water	11.3
	O1s − 2	531.72	Bulk hydroxyls	88.7
	Al2p − 1	74.20	Gibbsite Al2p	100
Gibbsite γ-irradiated	O1s − 1	533.57	Adsorbed water	13.3
	O1s − 2	531.78	Bulk hydroxyls	86.7
	Al2p − 1	74.22	Gibbsite Al2p	100
Gibbsite α-irradiated	O1s − 1	531.60	Bulk hydroxyls	80.9
	O1s − 2	530.32	Bulk oxygen	13.3
	O1s − 3	528.85	??	5.8
	Al2p − 1	74.16	Gibbsite Al2p	86.2
	Al2p − 2	72.38	Aluminum metal	13.8
Boehmite Pristine	O1s − 1	533.90	Adsorbed water	13.6
	O1s − 2	532.14	Bulk hydroxyls	70.1
	O1s − 3	530.83	Bulk oxygen	16.3
	Al2p − 1	74.56	Boehmite Al2p	100
Boehmite γ-irradiated	O1s − 1	533.94	Adsorbed water	10.1
	O1s − 2	532.20	Bulk hydroxyls	63.7
	O1s − 3	530.87	Bulk oxygen	26.2
	Al2p − 1	74.39	Boehmite Al2p	100
Boehmite α-irradiated	O1s − 1	532.14	Bulk hydroxyls	43.4
	O1s − 2	530.74	Bulk oxygen	48.9
	O1s − 3	528.88	??	7.7
	Al2p − 1	74.30	Boehmite Al2p	88.5
	Al2p − 2	72.41	Aluminum metal	11.5

The plate-like gibbsite and boehmite particles are 200–400 nm and 20–80 nm, respectively, with a thickness of 10–30 nm. The penetration depth of the X-rays at the Al K-edge in Al oxides is ~40 nm; however, given data collection in TEY mode and signal current dominated by Auger electron emission that rapidly decays exponentially into particle interiors, by design the XANES/EXAFS spectra report primarily on just the upper few angstroms of the particle surfaces. Fig. 9 shows the Al K-edge XANES, EXAFS and Fourier transform of the EXAFS data for gibbsite before and after irradiation at 0.5 MGy, 1.0 MGy and 2.0 MGy. Although the XANES spectra for the samples are similar, a shoulder develops systematically with dose on the low energy side of the main peak (see Fig. 9A, inset). This peak could be due to oxygen-centered defect (O^-) production at the $Al(OH)_3$ surface, as similar centers are formed in Al_2O_3 nanoparticles by dehydration [5], and the energy of the excited state for O^- is expected to be lower than that for O^{2-}. Vjunov et al. also noted a change in length of the Al-O bonds causes distortion of the symmetry, leading to a lower energy pre-edge feature in the AL K-edge XANES spectrum [25]. The EXAFS and the Fourier transform of the EXAFS data (Fig. 9B and C) do not change with irradiation, confirming that there are no structural changes because of gamma irradiation, in agreement with the XRD data.

Fig. 10 shows the O K-edge spectra for gibbsite before and after irradiation. There are three distinguishable peaks at 532, 535 and 540 eV. The first peak at 532 eV decreases with dose and could be due to adsorbed O_2 that is removed during irradiation. The peaks at 535 eV and 540 eV are assigned to σ* transitions of Al–O and O–H bonding [26]. Although there are differences between the spectra, no trend between the ratio of OH^- to O^{2-} as a function of radiation dose can be discerned.

Fig. 11 shows the Al K-edge XANES, EXAFS and Fourier transform of the EXAFS data for boehmite before and after irradiation at 0.5 MGy and 2.0 MGy. As with gibbsite, a low energy shoulder on the main peak develops systematically with dose (see Fig. 11A, inset), also likely due to oxygen-centered defect (O^-) production. Again, there is no evidence for radiation-induced structural

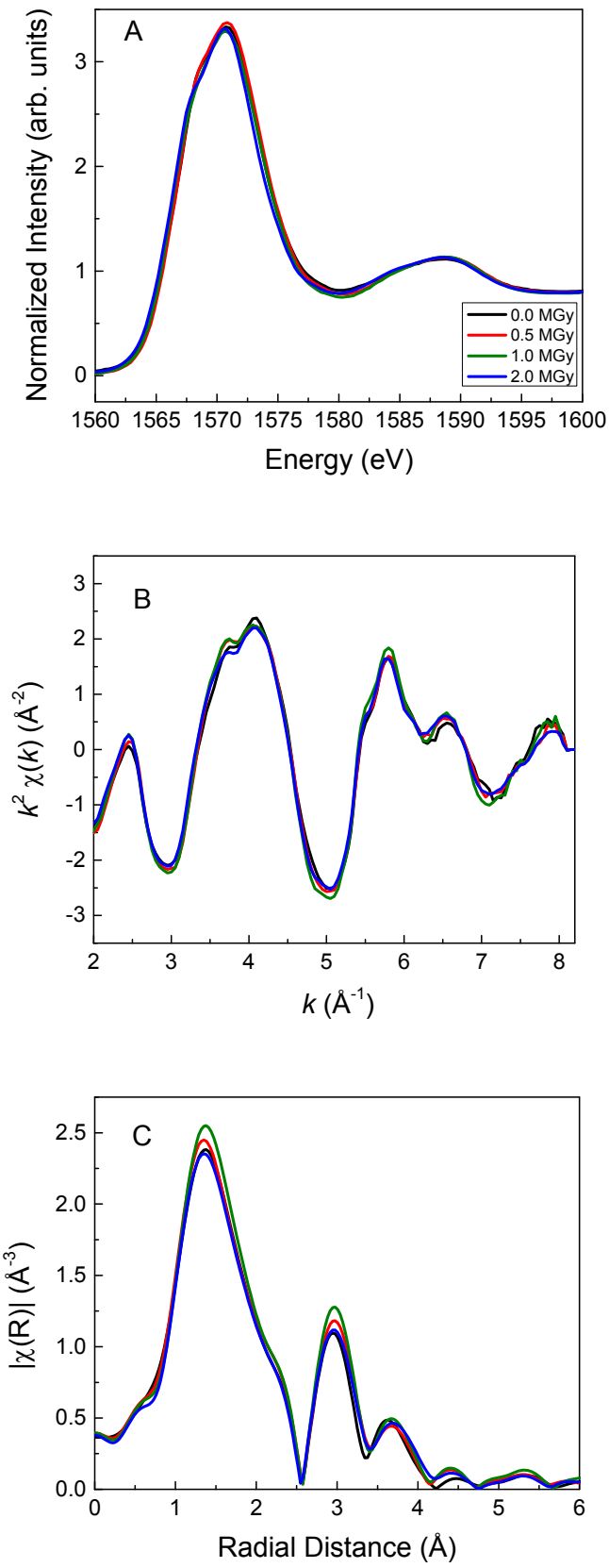

Fig. 9. Al K-edge XANES (A), EXAFS (B) and Fourier transform of the EXAFS data (C) for gibbsite before and after irradiation at 0.5, 1.0 and 2.0 MGy.

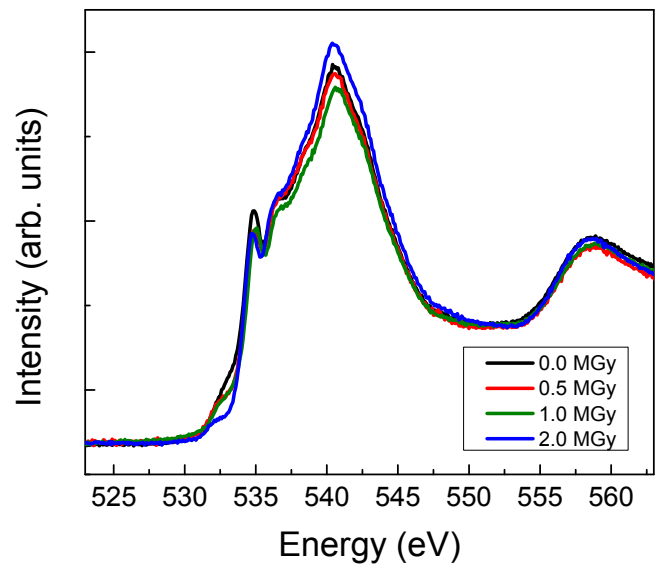

Fig. 10. O K-edge X-ray absorption spectra for gibbsite before and after irradiation at 0.5, 1.0, and 2.0 MGy.

changes as the EXAFS and the Fourier transform of the EXAFS data (Fig. 11B and C) do not change.

In contrast to gibbsite, the O K-edge spectrum shown in Fig. 12 for boehmite did not change significantly before and after irradiation, suggesting that: (i) there is little to no adsorbed O_2 on the surface of the boehmite; and (ii) the OH^- in the structure is perhaps more susceptible to radiation effects, and there is one third the amount of these groups per Al atom in boehmite (AlOOH) than in gibbsite ($Al(OH)_3$).

Although the Al K-edge EXAFS data for both gibbsite and boehmite confirmed that there is no detectable change in the structure as a result of γ-irradiation up to 2 MGy, it is interesting to note that irradiation did have a significant effect on the charging properties of the samples with the energy position of the Al K-edge peak for both gibbsite and boehmite shifted to lower energy by ~1 eV after irradiation. This effect can be seen in the spectra prior to energy calibration using the Si peak at 1839 eV.

4. Conclusions

Water is chemisorbed at sites that are very similar in energy on both boehmite and gibbsite. Heating to 500 °C drives off most of the chemisorbed water but also converts both materials to an amorphous state. Boehmite appears to pass through a state similar to alumina before becoming amorphous, while the transformation of gibbsite is too complete to observe any intermediate state. No variation in overall phase or crystallinity due to radiolysis of both compounds was observed with XRD and Raman spectroscopy for doses up to 2 MGy with γ-rays and 175 MGy with α-particles. Although γ-rays did not result in structural changes to the particles, analysis using Al K-edge XANES spectroscopy revealed significant energy shifts due to charging after irradiation and subtle changes in the shape of the spectra due to formation of electronic defects. XPS indicates surface reduction of Al(III) to Al metal on radiolysis with α-particles. Complete loss of chemisorbed water and the formation of bulk O atoms was observed following radiolysis with α-particles.

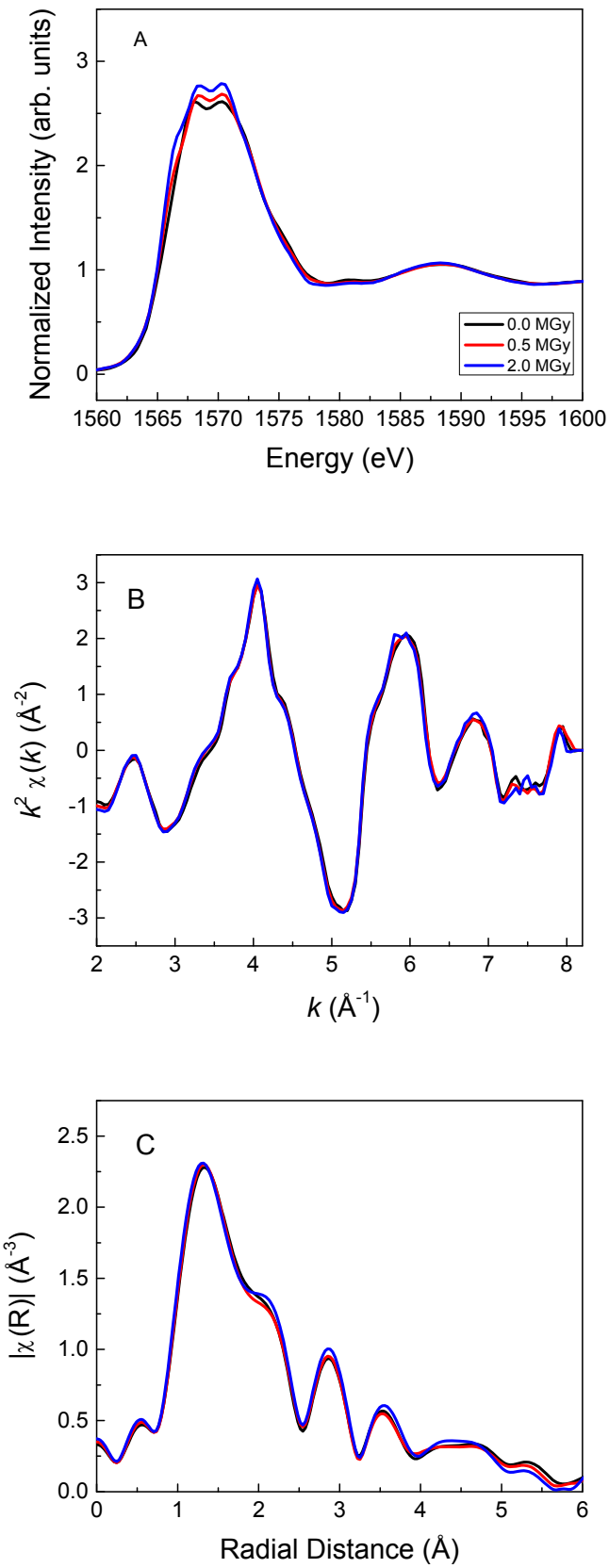

Fig. 11. Al K-edge XANES (A), EXAFS (B) and Fourier transform of the EXAFS data (C) for boehmite before and after irradiation at 0.5 and 2.0 MGy.

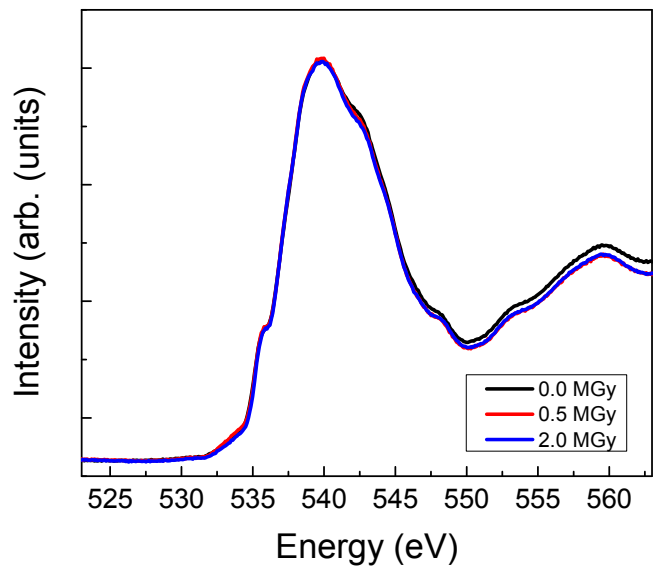

Fig. 12. O K-edge X-ray absorption spectra for boehmite before and after irradiation at 0.5 MGy and 2.0 MGy.

Acknowledgments

This majority of this work was supported by IDREAM (Interfacial Dynamics in Radioactive Environments and Materials), an Energy Frontier Research Center funded by the U.S. Department of Energy, Office of Science, Office of Basic Energy Sciences (BES). The authors acknowledge the Center for Sustainable Energy at Notre Dame (cSEND) Materials Characterization Facilities for the use of the PHI VersaProble II X-ray Photoelectron Spectrometer, Jasco Micro-Raman Spectrometer NRS-5100, and Bruker D8 Advance Davinci Powder X-ray Diffractometer and the Notre Dame Integrated Imaging Facility (NDIFF) for the use of the Magellan 400 FESEM. Support of the National Science Foundation through MRI award 1126374 is acknowledged for the XPS data in this paper. The work performed at the Advanced Light Source (ALS) was supported by the Office of Science BES of the DOE under Contract No. DE-AC02-05CH11231. Materials synthesis was performed using EMSL, a national scientific user facility sponsored by the DOE Office of Biological and Environmental Research and located at Pacific Northwest National Laboratory. PNNL is a multiprogram national laboratory operated for DOE by Battelle Memorial Institute under Contract No. DE-AC06-76RLO-1830. The authors thank Prof. Michael Wiescher for making available the facilities of the Notre Dame Nuclear Science Laboratory, which is supported by the U.S. National Science Foundation through grant number Phys-0758100, and Prof. Ian Carmichael for making available the facilities of the Notre Dame Radiation Laboratory, which is supported by DOE BES through grant number DE-FC02-04ER15533. This contribution is NDRL-5195 from the Notre Dame Radiation Laboratory.

Appendix A. Supplementary data

Supplementary data related to this article can be found at https://doi.org/10.1016/j.jnucmat.2018.01.043.

References

[1] Y.S. Kim, G.L. Hofman, A.B. Robinson, J.L. Snelgrove, N. Hanan, Oxidation of aluminum alloy cladding for research and test reactor fuel, J. Nucl. Mater. 378 (2009) 220–228.

[2] J.G. Reynolds, J.K. McCoskey, D.L. Herting, Gibbsite solubility in hanford nuclear waste approached from above and below saturation, Ind. Eng. Chem. Res. 55 (2016) 5465–5473.

[3] A.A. Akatov, B.S. Nikonov, B.I. Omel'yanenko, O.I. Stefanovskaya, S.V. Stefanovsky, D.Y. Suntsov, J.C. Marra, Influence of the content of a surrogate of iron aluminate high-level wastes on the phase composition and structure of glassy materials for their immobilization, Glass Phys. Chem. 36 (1) (2010) 45–52.

[4] H. Li, P. Hrma, J.D. Vienna, M.X. Qian, Y.L. Su, D.E. Smith, Effects of Al_2O_3, B_2O_3, Na_2O, and SiO_2 on nepheline formation in borosilicate glasses: chemical and physical correlations, J. Non-Cryst. Solids 331 (1–3) (2003) 202–216.

[5] J.A. Kaddissy, S. Esnouf, D. Durand, D. Saffre, E. Foy, J.P. Renault, Radiolytic events in nanostructured aluminum hydroxides, J. Phys. Chem. C 121 (11) (2017) 6365–6373.

[6] M.L. Westbrook, R.L. Sindelar, D.L. Fisher, Radiolytic hydrogen generation from aluminum oxyhydroxide solids: theory and experiment, J. Radioanal. Nucl. Chem. 303 (2015) 81–86.

[7] S.C. Reiff, J.A. LaVerne, Radiolysis of water with aluminum oxide surfaces, Radiat. Phys. Chem. 131 (2017) 46–50.

[8] W.J. Weber, R.C. Ewing, C.R.A. Catlow, T.D. de la Rubia, L.W. Hobbs, C. Kinoshita, H. Matzke, A.T. Motta, M. Nastasi, E.K.H. Salje, E.R. Vance, S.J. Zinkle, Radiation effects in crystalline ceramics for the immobilization of high-level nuclear waste and plutonium, J. Mater. Res. 13 (6) (1998) 1434–1484.

[9] X. Zhang, X.-W. Zhang, T.R. Graham, C.I. Pearce, B.L. Mehdi, A. N'Diaye, S. Kerisit, N.D. Browning, S.B. Clark, K.M. Rosso, Fast synthesis of gibbsite nanoplates and process optimization using box-behnken experimental design, Cryst. Growth Des. 17 (12) (2017) 6801–6808.

[10] A. Erbil, G.S. Cargill, R. Frahm, R.F. Boehme, Total electron-yield-current measurements for near-surface extended x-ray-absorption fine-structure, Phys. Rev. B 37 (1988) 2450–2465.

[11] P. Ildefonse, D. Cabaret, P. Sainctavit, G. Calas, A.M. Flank, P. Lagarde, Aluminum x-ray absorption near edge structure in model compounds and Earth's surface minerals, Phys. Chem. Miner. 25 (1998) 112–121.

[12] B. Ravel, M. Newville, ATHENA, ARTEMIS, HEPHAESTUS; data analysis for x-ray absorption spectroscopy using IFEFFIT, J. Synchrotron Radiat. 12 (2005) 537–541.

[13] J.F. Ziegler, J.P. Biersack, U. Littmark, The Stopping and Range of Ions in Solids, Pergamon, New York, 1985.

[14] H.D. Ruan, R.L. Frost, J.T. Kloprogge, Comparison of Raman spectra in characterizing gibbsite, bayerite, diaspore and boehmite, J. Raman Spectrosc. 32 (9) (2001) 745–750.

[15] J. Zhang, H.-T. Li, J.-H. Guo, F.-R. Hu, Raman scattering modification induced by structural change in alumina polymorphs, Chin. Phys. Lett. 32 (2015) 1268011–1268014.

[16] H.P. Boehm, Acidic and basic properties of hydroxylated metal oxide surfaces, Discuss. Faraday Soc. 52 (0) (1971) 264–275.

[17] R.L. Frost, J.T. Kloprogge, S.C. Russell, J. Szetu, Dehydroxylation of aluminum (oxo)hydroxides using infrared emission spectroscopy. Part II: boehmite, Appl. Spectrosc. 53 (5) (1999) 572–582.

[18] R.L. Frost, J.T. Kloprogge, S.C. Russell, J.L. Szetu, Vibrational spectroscopy and dehydroxylation of aluminum (oxo)hydroxides: gibbsite, Appl. Spectrosc. 53 (4) (1999) 423–434.

[19] S. Louaer, Y. Wang, L. Guo, Fast synthesis and size control of gibbsite nanoplatelets, their pseudomorphic dehydroxylation, and efficient dye adsorption, Appl. Mater. Interfaces 5 (2013) 9648–9655.

[20] J.T. Kloprogge, H.D. Ruan, R.L. Frost, Thermal decomposition of bauxite minerals: infrared emission spectroscopy of gibbsite, boehmite and diaspore, J. Mater. Sci. 37 (6) (2002) 1121–1129.

[21] P.A. Redhead, Thermal desorption of gases, Vacuum 12 (4) (1962) 203–211.

[22] M.D. Dyar, C.A. Hibbitts, T.M. Orlando, Mechanisms for incorporation of hydrogen in and on terrestrial planetary surfaces, Icarus 208 (1) (2010) 425–437.

[23] J.T. Kloprogge, L.V. Duong, B.J. Wood, R.L. Frost, XPS study of the major minerals in bauxite: gibbsite, bayerite and (pseudo-)boehmite, J. Colloid Interface Sci. 296 (2) (2006) 572–576.

[24] K. Konstadinidis, B. Thakkar, A. Chakraborty, L.W. Potts, R. Tannenbaum, M. Tirrell, J.F. Evans, Segment level chemistry and chain conformation in the reactive adsorption of poly(methyl methacrylate) on aluminum oxide surfaces, Langmuir 8 (5) (1992) 1307–1317.

[25] A. Vjunov, M. Wang, N. Govind, T. Huthwelker, H. Shi, D. Mei, J.L. Fulton, J.A. Lercher, Tracking the chemical transformations at the bronsted acid site upon water-induced deprotonation in a zeolite pore, Chem. Mater. 29 (21) (2017) 9030–9042.

[26] Y.F. Hu, R.K. Xu, J.J. Dynes, R.I.R. Blyth, G. Yu, L.M. Kozak, P.M. Huang, Coordination nature of aluminum (oxy)hydroxides formed under the influence of tannic acid studied by X-ray absorption spectroscopy, Geochem. Cosmochim. Ac. 72 (2008) 1959–1969.